Characterizing and Overcoming Surface Paramagnetism in Magnetoelectric Antiferromagnets

Sophie F. Weber and Nicola A. Spaldin
Materials Theory, ETH Zürich, Wolfgang-Pauli-Strasse 27, 8093 Zürich, Switzerland

(Received 29 August 2022; revised 23 January 2023; accepted 16 March 2023; published 4 April 2023)

We use a combination of density functional theory and Monte Carlo methods to calculate the surface magnetization in magnetoelectric Cr_2O_3 at finite temperatures. Such antiferromagnets, lacking both inversion and time-reversal symmetries, are required by symmetry to possess an uncompensated magnetization density on particular surface terminations. Here, we first show that the uppermost layer of magnetic moments on the ideal (001) surface remains paramagnetic at the bulk Néel temperature, bringing the theoretical estimate of surface magnetization density in line with experiment. We demonstrate that the lower surface ordering temperature compared to bulk is a generic feature of surface magnetization when the termination reduces the effective Heisenberg coupling. We then propose two methods by which the surface magnetization in Cr_2O_3 could be stabilized at higher temperatures. Specifically, we show that the effective coupling of surface magnetic ions can be drastically increased either by a different choice of surface Miller plane, or by Fe doping. Our findings provide an improved understanding of surface magnetization properties in AFMs.

DOI: 10.1103/PhysRevLett.130.146701

Magnetoelectric (ME) antiferromagnets (AFMs) acquire a net magnetization $\mathbf{M}$ in response to an applied electric field $\mathbf{E}$, and conversely, a net electric polarization $\mathbf{P}$ in response to an applied magnetic field $\mathbf{H}$ [1]. For the linear ME effect to manifest, an AFM must lack both inversion and time-reversal symmetries. This implies another intriguing property of ME AFMs; namely, certain surfaces must have a finite magnetic dipole per unit area [2], which we refer to as "surface magnetization" throughout this Letter. Such surface magnetization has promising device applications, since the ME effect allows the bulk domain to be readily switched using electric fields in a constant magnetic field [3], and the direction of surface magnetization, which couples to the bulk Néel vector, can be directly detected [4]. Additionally, surface magnetization plays a role in exchange bias coupling, exploited in magnetic storage devices to pin the magnetization orientation of a ferromagnet (FM) by an adjacent AFM [5,6].

An important question about surface magnetism is its degree of disorder close to the bulk Néel temperature T_N^{bulk}, near which relevant devices typically operate. Indeed, in the case of Cr_2O_3 (chromia), a ME AFM viewed as a promising spintronics candidate due to its relatively high Néel temperature ~300 K [3,7–9] (which can be increased further with boron doping [10]), theoretical predictions assuming that bulk AFM order persists at the surface overestimate the (001) surface magnetization measured using nitrogen vacancy magnetometry [11–13]. This discrepancy is resolved if the surface Cr moments are disordered at room temperature [13]. A better understanding of the temperature dependence of surface magnetization in AFMs would facilitate quantitative comparison between theory and experiment, and could inform design of related spintronics devices.

In this Letter, we use density functional theory (DFT) and Monte Carlo (MC) calculations to explore the temperature dependence of surface magnetism, taking Cr_2O_3 as an example. We show that partial to full disorder is a generic property of surface magnetization around T_N^{bulk} when surface magnetic moments have fewer or smaller magnetic interactions than the bulk. We then propose two promising options for stabilizing the surface magnetization of Cr_2O_3 at higher temperatures, first by using a Miller plane with magnetic coupling close to bulk, and secondly by depositing an Fe monolayer on the (001) surface.

We first restate two key concepts, discussed in detail elsewhere [13,14]. The first regards the construction of an electrostatically stable, nonpolar surface termination for a given Miller plane (h, k, l) [14]. A stable surface has no bound charge, since finite σ_{surf} implies a diverging electrostatic potential [15]. σ_{surf} is determined by the component of bulk electric polarization $\mathbf{P}_{\text{bulk}}$ perpendicular to the surface [16]: $\mathbf{P}_{\text{bulk}} \cdot \hat{\mathbf{n}} = \sigma_{\text{surf}}$, where $\hat{\mathbf{n}}$ is the unit surface normal and $\mathbf{P}_{\text{bulk}}$ is the polarization of the unit cell which periodically tiles the semi-infinite solid containing the surface of interest. Thus, a stable surface plane has $\mathbf{P}_{\text{bulk}} \cdot \hat{\mathbf{n}} = \sigma_{\text{surf}} = 0$.

Second, we point out the connection between the bulk ME multipolization tensor and surface magnetization [13]. The multipolization tensor is defined as $\mathcal{M}_{ij} = 1/V \int r_i \boldsymbol{\mu}_j(\mathbf{r}) d^3\mathbf{r}$,

where r_i is the ith Cartesian position component, $\mu_j(\mathbf{r})$ is the jth magnetization density component at $\mathbf{r}$, and V is the unit cell volume. $\mathcal{M}$ describes first-order asymmetry in $\mu(\mathbf{r})$ beyond the magnetic dipole [17]. For materials in which $\mu(\mathbf{r})$ is localized around magnetic ions, $\mathcal{M}_{ij}$ can be approximated by

$$\mathcal{M}_{ij} = \frac{1}{V}\sum_{\alpha} r_i^{\alpha} m_j^{\alpha}, \tag{1}$$

where the sum is over magnetic ions in the unit cell, and $\mathbf{m}^{\alpha}$ is the magnetic dipole moment of atom α.

The requirements for $\mathcal{M}$ to have nonzero components, that is, broken inversion and time-reversal symmetries, are identical to those for a nonzero linear ME response. Introducing a surface reduces symmetry in the same way as applying an electric field in bulk; therefore, ME AFMs have nonzero surface magnetization [2,13,18]. Analogously to the surface charge density resulting from bulk polarization, the bulk multipolization tensor $\mathcal{M}$, calculated from Eq. (1) for the unit cell which tiles the semi-infinite solid containing the surface, gives rise to a surface magnetization μ_{surf} [13], where component $\mathcal{M}_{ij}$ gives the $\hat{j}$-oriented dipole moment per unit area on a surface with normal $\hat{i}$. Given a specific plane and atomic termination, the three multipolization components and thus the surface magnetization corresponding to the surface normal $\hat{i}$ are fixed, assuming bulklike surface moments.

Results and discussion.—Cr_2O_3 crystallizes in the corundum structure with magnetic space group $R\bar{3}'c'$ [19]. Figure 1(a) shows the 12-Cr unit cell in the hexagonal setting. Bulk Cr_2O_3 adapts an "up down up down" ordering of the Cr magnetic moments along [001] as shown in Fig. 1(b). This magnetic ground state is well described [20,21] by a Heisenberg Hamiltonian,

$$\mathcal{H}_{\text{Heis}} = -\sum_{\langle i,j\rangle} J_{i,j}(\mathbf{e}_i \cdot \mathbf{e}_j), \tag{2}$$

that includes coupling up to fifth-nearest neighbor interactions, where $\mathbf{e}_i$ is the unit vector parallel to the magnetic moment of the Cr ion at site i, and $J_{i,j}$ is the coupling constant between sites i and j. J_1–J_5, where J_n denotes the coupling for the nth nearest neighbor, are depicted in Fig. 1(a). Quantitative values of J_1–J_5 for bulk Cr_2O_3, which we calculate using first-principles DFT + U as implemented in VASP [22], are given in Table I [23]. Our values agree with previous calculations using similar parameters [21]. The magnetism is dominated by AFM J_1 and J_2 couplings.

We first review magnetism on the (001) surface of vacuum-terminated chromia. The bulk unit cell with a single terminating Cr on the left of Fig. 1(b) defines the nonpolar (001) surface according to $\mathbf{P}_{\text{bulk}} = 1/V\sum_i Z_i \mathbf{r}_i$,

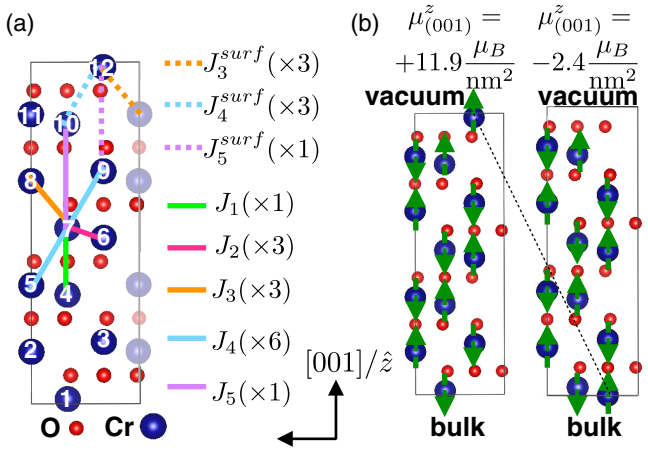

FIG. 1. (a) Unit cell of Cr_2O_3 with nearest-neighbor Heisenberg couplings indicated for bulk (solid lines) and (001) surface Cr's (dashed lines). Numbers in parentheses indicate coupling degeneracies. Lighter colored atoms are in the adjacent unit cell. White numbers label the 12 Cr in the (001) slab. (b) Left: unit cell defining the nonpolar (001) surface with ground state AFM order. Right: unit cell for calculating surface magnetization if the top moment of the nonpolar surface is disordered.

where Z_i is the formal ionic charge (+3 and −2 for Cr and O, respectively), and $\mathbf{r}_i$ the position of atom i in the unit cell. If we assume all Cr magnetic moments point along [001] with bulk AFM order, using the formal value 3 μ_B for Cr^{3+} and the Cr positions in the hexagonal cell [23], Eq. (1) yields a $+\hat{z}/[001]$-oriented (001) surface magnetization of 11.9 μ_B/nm^2 for the magnetic domain depicted (all other multipolization tensor components are zero within the local moment approximation; small (1,1) and (2,2) components are symmetry-allowed if one use the exact integral form [38]). The energetically equivalent AFM domain with reversed magnetic moments has a value of equal magnitude and opposite sign.

As mentioned previously, this predication overestimates measurements of (001) Cr_2O_3 surface magnetism using scanning nitrogen vacancy magnetometry [11,12], which are consistent with values between 1.6 to 2.3 μ_B/nm^2. Recall, however, that the 11.9 μ_B/nm^2 value is calculated assuming that all Cr magnetic moments are completely along [001]. The outermost Cr for the nonpolar termination in Fig. 1(a) lacks J_1 and J_2 nearest neighbors, only retaining smaller J_3-J_5 couplings. From a mean-field argument, the ordering temperature for a magnetic moment at site i is proportional to $\lambda_J^i S_i$ [39], where S_i is the spin value and the total effective coupling for site i is

$$\lambda_J^i = \sum_j J_{ij} \times (\hat{e}_i \cdot \hat{e}_j). \tag{3}$$

Using the J values in Table I calculated for bulk Cr_2O_3, λ_J for a bulk Cr spin is $\lambda_J^{\text{bulk}} = -J_1 - 3J_2 - 3J_3 + 6J_4 - J_5 = 40.25$ meV, whereas the Cr on the (001)

TABLE I. Heisenberg coupling constants, degeneracies in parentheses, and effective coupling λ_J^i calculated for bulk Cr_2O_3, for Cr on the (001) surface (using bulk and structurally relaxed values, respectively), for Cr on a $(\bar{1}02)$ surface, and Cr-Fe couplings for (001) Cr_2O_3 with an Fe monolayer.

	Bulk	(001) Surface (bulk)	(001) Surface (relaxed)	$(\bar{1}02)$ Surface (bulk)	$(\bar{1}02)$ Surface (relaxed)	Fe on (001) (relaxed)
J_1 (meV)	−10.46 (1)	⋯	⋯	−10.46 (1)	−17.16 (1)	⋯
J_2 (meV)	−7.88 (3)	⋯	⋯	−7.88 (2)	−9.42 (2)	⋯
J_3 (meV)	+0.86 (3)	+0.86 (3)	−0.15 (3)	+0.86 (1)	+0.43 (1)	−30.81 (3)
J_4 (meV)	+1.22 (6)	+1.22 (3)	+4.44 (3)	+1.22 (5)	$+0.43^a$ (4)/ $+3.40^b$ (1)	−19.77 (3)
J_5 (meV)	−1.41 (1)	−1.41 (1)	−0.39 (1)	⋯	⋯	−3.63 (1)
λ_J (meV)	40.25	2.48	14.18	31.47	40.16	155.33

surface [Cr 12 in Fig. 1(a)] has $\lambda_J^{\text{surf}} = -3J_3 + 3J_4 - J_5 = 2.48$ meV. Thus, $\lambda_J^{\text{surf}}/\lambda_J^{\text{bulk}} = 0.06$, implying that for the $T = 295$ K magnetometry measurements, just below $T_N^{\text{bulk}} \sim 300$ K, the surface Cr should be largely paramagnetic. Given this magnetic dead layer (which occurs even for an idealized, atomically-smooth (001) surface), a more appropriate basis for predicting surface magnetization is that shown on the right of Fig. 1(b), corresponding to displacing the surface magnetic moment downwards by one **c** lattice vector. Recalculating the (3,3) component of $\mathcal{M}$ using the Cr positions of this new unit cell [23] yields $\mu_{(001)}^z = -2.4\ \mu_B/\text{nm}^2$, in line with experiment. Note that this is an upper bound, since near T_N^{bulk} the bulk moments also deviate marginally from complete [001] alignment.

To confirm our analysis, we examine the temperature dependence of magnetization for a [001]-oriented Cr_2O_3 slab with Monte Carlo (MC) simulations as implemented in UPPASD [23,40]. We enforce in-plane periodic boundary conditions and vacuum boundary conditions along [001]. Figure 2(a) shows the normalized magnitude of the $[001]/\hat{z}$ component of bulk sublattice magnetization as a function of temperature, calculated by averaging m_z of the sixth Cr sublattice in the center of our unit-cell thick slab, compared to the averaged m_z of the terminating Cr's on the (001) surface. While both become nonzero at T_N^{bulk}, their approaches to T_N^{bulk} are different: the "bulk" Cr sublattice exhibits the normal Langevin-like $m_z^{\text{sub}}(T)$ behavior, but the surface magnetization falls off rapidly with increasing temperature and is negligible just below T_N^{bulk}, consistent with earlier DFT-MC calculations [41]. Note that our calculated couplings lead to a significant underestimate of T_N^{bulk}; this has been observed in previous DFT-MC calculations of Cr_2O_3 and we discuss the origin of the underestimation further in the Supplemental Material [23,42]. While $m_z(T)$ in Fig. 2(a) for both surface and bulk Cr's is computed using the DFT J values calculated with bulk Cr_2O_3, atomic relaxation can lead to significant renormalization of the surface couplings. The third column of Table I shows the values of J_3–J_5 for the surface Cr computed using a [001] vacuum-terminated 12-Cr-thick slab structurally relaxed within DFT. The modified effective coupling for the surface Cr is $\lambda_J^{\text{surf,relaxed}} = 14.2$ meV. Figure 2(b) shows $m_z^{\text{sub}}(T)$ for the surface Cr with these relaxed values. While $m_z^{\text{sub,surf}}$ is still mostly disordered just below T_N^{bulk}, the increased λ_J^{surf} leads to a roughly linear decrease of $m_z^{\text{sub,surf}}$ with increasing T, as opposed to the exponential-like falloff in Fig. 2(a). This temperature dependence could likely be probed with magnetotransport measurements, given the short spin decay length of Cr_2O_3 [43].

To determine the detailed dependence of the surface magnetism on λ_J^{surf}, we next vary λ_J^{surf} in the MC simulations by setting all other surface couplings to zero except for $J_4^{\text{surf}} = \lambda_J^{\text{surf}}/3$. For each value of λ_J^{surf} we calculate $m_{\text{surf}}^{z,\text{sub}}/m_{\text{bulk}}^{z,\text{sub}}$ at $T = 100$ K; the result is plotted in Fig. 3. We choose 100 K as a representative temperature because

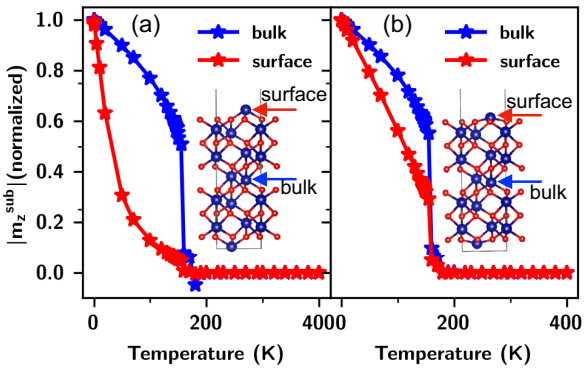

FIG. 2. (a) Normalized sublattice magnetization along $\hat{z}/[001]$ versus temperature for a bulk Cr in the center of a [001]-oriented slab, and for the surface Cr. Here the couplings calculated from bulk Cr_2O_3 are used for both surface and bulk Cr moments. (b) m_z^{sub} using couplings calculated from a relaxed slab for the surface Cr.

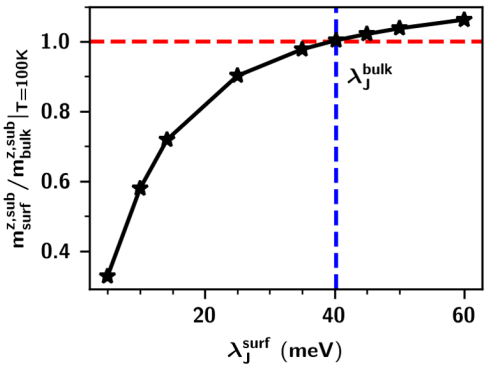

FIG. 3. Ratio of $m_{\text{surf}}^{z,\text{sub}}$ to $m_{\text{bulk}}^{z,\text{sub}}$ at $T = 100$ K ($\sim T_N^{\text{bulk}}/2$) versus λ_J^{surf}. The dashed blue line indicates λ_J^{bulk}.

it is roughly $T_N^{\text{bulk}}/2$ (due to the finite slab size, $T_N^{\text{bulk}}/2$ depends negligibly on λ_J^{surf}). $(m_{\text{surf}}^{z,\text{sub}}/m_{\text{bulk}}^{z,\text{sub}})|_{T=100\text{ K}}$ increases monotonically with λ_J^{surf} and matches the bulk sublattice magnetization $[(m_{\text{surf}}^{z,\text{sub}}/m_{\text{bulk}}^{z,\text{sub}}) = 1]$ roughly when λ_J^{surf} equals λ_J^{bulk} (dashed blue line). Therefore, by engineering λ_J^{surf} to be close to λ_J^{bulk}, one obtains bulklike temperature dependence of surface magnetization. Moreover, if the Heisenberg J's for a material are known, one can estimate from λ_J^{surf} how much $m_{\text{surf}}^{\text{sub}}$ is likely to be reduced relative to $m_{\text{bulk}}^{\text{sub}}$. Beyond this Letter's focus, tuning both bulk and surface $m^{\text{sub}}(T)$ and the corresponding critical exponents by modifying λ_J is a broadly applicable strategy to enhance material tunability in both FMs and AFMs [44]. We now discuss two approaches, also applicable to other ME AFMs, for stabilizing surface magnetization in Cr_2O_3 at higher temperatures. The first is simply to use a surface corresponding to a different Miller plane for which λ_J^{surf} is close to λ_J^{bulk}. We demonstrate this for Cr_2O_3. Figure 4(a) shows the unit cell corresponding to the nonpolar termination of a $(\bar{1}02)$ surface, which has a large λ_J^{surf} and a non-negligible theoretical surface magnetization density. Specifically, for the domain shown, Eq. (1) predicts an out-of-plane (in-plane) magnetization component of $-4.75\ \mu_B/\text{nm}^2$ ($+7.55\ \mu_B/\text{nm}^2$), respectively, on the $(\bar{1}02)$ surface [23].

The couplings and degeneracies, shown in Fig. 4(b), retained by the outermost Cr and corresponding λ_J^{surf} for the $(\bar{1}02)$ surface are given in Table I both with DFT values calculated from bulk Cr_2O_3 and with surface couplings calculated from a relaxed $(\bar{1}02)$ slab. The a and b superscripts refer to the J_4 couplings in Fig. 4(b) which become inequivalent upon relaxation. λ_J^{surf} is 31.47 (40.16) meV for bulk (relaxed) coupling values on the $(\bar{1}02)$ surface. Even using the bulk values, the surface magnetization is nearly bulklike, and with the relaxed values leading to $\lambda_J^{\text{surf}} \sim \lambda_J^{\text{bulk}}$, bulk and $(\bar{1}02)$ surface $m_z^{\text{sub}}(T)$ lie on top of each other [Fig. 4(c)].

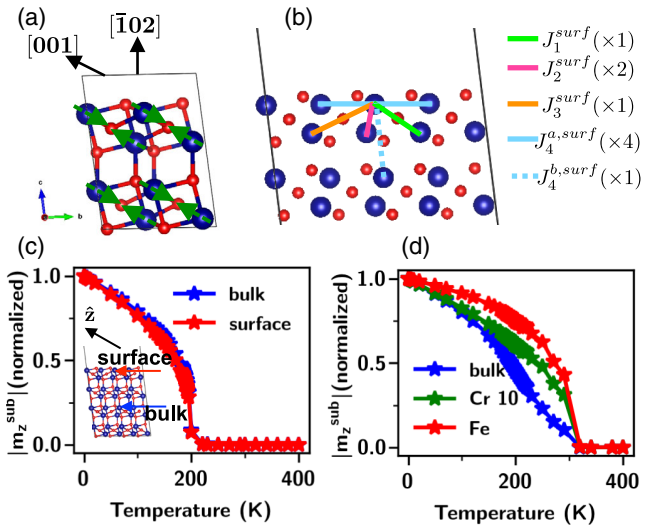

FIG. 4. (a) Bulk unit cell defining nonpolar $(\bar{1}02)$ surface of Cr_2O_3. (b) Heisenberg couplings for Cr on the $(\bar{1}02)$ surface. (c) $|m_z^{\text{sub}}(T)|$ (with z along the [001] easy axis) for Cr in bulk and on a $(\bar{1}02)$ surface (using relaxed surface couplings). (d) $|m_z^{\text{sub}}(T)|$ for Fe, Cr 10, and a central bulk Cr for (001) Cr_2O_3 with an Fe monolayer.

Extensive research has been devoted to the application of (001) Cr_2O_3 films in spintronic memory devices, where the AFM bulk domain serves as a logical bit whose direction can be read out by the sign of the surface magnetization (determined indirectly via the sign of the exchange bias field in an adjacent FM [3,18,45]). Our results imply that magnetism on the $(\bar{1}02)$ surface in chromia is strongly coupled to the bulk AFM domain, even at T_N^{bulk}, in contrast to the (001) surface, which is essentially paramagnetic at room temperature. Thus, a Cr_2O_3-based device with a $(\bar{1}02)$ rather than (001) surface plane might be a more robust option for memory applications. More fundamentally, a comparison of exchange bias properties of (001) and $(\bar{1}02)$ surfaces could shed light on the underlying mechanism.

Our second proposal for stabilizing surface magnetization involves chemical substitution. We take the Cr_2O_3 (001) surface, and deposit a monolayer of Fe, substituting the 12th Cr in Fig. 1(a). Since Fe adopts a 3+ valence state, this structure is nonpolar [23]. Crucially, while Cr-Cr J_3–J_5 are negligible compared to J_1 and J_2, prior DFT studies using a Cr_2O_3-Fe_2O_3 heterostructure indicate that the J_3 and J_4 Cr-Fe couplings are tens of meV [46]. The differences in strengths and signs of Cr-Cr and Cr-Fe couplings are attributed to the relative $e_g - t_{2g}$ occupation of the Cr^{3+} (t_{2g}^3, e_g^0) and Fe^{3+} (t_{2g}^3, e_g^2) ions, combined with the coupling angles via oxygen [42]. In the final column of Table I, we show our results for the surface Fe-Cr couplings calculated using a relaxed Cr_2O_3 slab terminated on one side with Fe. $J_3^{\text{surf,Cr-Fe}}$ and $J_4^{\text{surf,Cr-Fe}}$ are even larger than the $J_1^{\text{Cr-Cr}}$ and $J_2^{\text{Cr-Cr}}$ dominant in Cr_2O_3 bulk.

Figure 4(d) shows $|m_z^{\mathrm{sub}}(T)|$ for the surface Fe monolayer and center Cr bulk, as well as for "Cr 10" [labeling in Fig. 1(a)] which couples to Fe via $J_4^{\mathrm{surf,Fe\text{-}Cr}}$ (Cr 10 reverses its orientation compared to that in pristine Cr_2O_3 due to this strong AFM $J_4^{\mathrm{surf,Fe\text{-}Cr}}$). From T_N^{bulk} until very low temperatures, the Cr ions coupled directly to the Fe monolayer have magnetization intermediate between the deeper bulk Cr and the Fe.

A notable feature of the surface magnetization in Fe-capped Cr_2O_3 in Fig. 4(d) is that $m_{\mathrm{Fe,surf}}^{z,\mathrm{sub}}$ (and $m_{\mathrm{Cr10}}^{z,\mathrm{sub}}$) increases more rapidly with decreasing temperature than the bulk Cr, making this an attractive test case for fundamental research in paramagnetic bulk materials with surface magnetic order [47–49]. Moreover, if scanning nitrogen vacancy magnetometry measurements could be compared at temperatures just above (where only Fe and the topmost Cr are fully ordered) and below T_N^{bulk}, monitoring surface magnetization changes would provide an indication of the technique's depth resolution.

In addition to stabilizing the surface magnetization just below T_N^{bulk}, Fig. 4(d) shows that an Fe monolayer increases the absolute value of T_N^{bulk}. Reciprocally, bulk modifications, such as boron doping [10,50,51], that raise T_N^{bulk} are likely to enhance the surface magnetization at room temperature. Graded doping could even be an effective strategy for engineering similar temperature dependencies for bulk and surface sublattices.

In summary, we have examined finite temperature properties of surface magnetization in ME AFMs using Cr_2O_3 as an example. Our DFT-MC calculations demonstrate that disorder of surface magnetic ions at T_N^{bulk} likely explains discrepancies between theoretical and experimental surface magnetization estimates for (001) Cr_2O_3. We have established a framework for assessing the relative ordering temperature of surface and bulk magnetization based on effective Heisenberg couplings. Finally, we have discussed two options for stabilizing surface magnetism, which would allow for higher temperature operation of relevant spintronic devices. We hope this Letter stimulates further theoretical studies, and that it motivates developments in the nitrogen vacancy magnetometry community, in particular temperature-dependent measurements, which will be essential in characterizing the detailed temperature dependence of surface magnetization in AFMs.

We thank Johan Hellsvik, Kirill Belashchenko, Xanthe Verbeek, Tara Tošić, Kai Wagner, Paul Lehman, Patrick Maletinsky, Sayantika Bhowal, and Andrea Urru for useful discussions. This work was funded by the ERC under the European Union's Horizon 2020 research and innovation program project HERO with Grant No. 810451. Calculations were performed at the Swiss National Supercomputing Centre (CSCS) under project number s889 and on the EULER cluster of ETH Zürich.

[1] D. N. Astrov, J. Exp. Theor. Phys. (U.S.S.R.) **11**, 984 (1960).
[2] K. D. Belashchenko, Phys. Rev. Lett. **105**, 147204 (2010).
[3] S. Ye, Phys. Status Solidi RRL **16**, 2100396 (2022).
[4] N. Hedrich, K. Wagner, O. V. Pylypovskyi, B. J. Shields, T. Kosub, D. D. Sheka, D. Makarov, and P. Maletinsky, Nat. Phys. **17**, 574 (2021).
[5] J. N. Nogue's and I. K. Schuller, J. Magn. Magn. Mater. **192**, 203 (1999).
[6] R. L. Stamps, J. Phys. D **33**, R247 (2000).
[7] W. Echtenkamp, Voltage-Controlled Magnetization in chromia-based magnetic heterostructures heterostructures, thesis, 2021, https://digitalcommons.unl.edu/physicsdiss.
[8] R. Schlitz, T. Kosub, A. Thomas, S. Fabretti, K. Nielsch, D. Makarov, and S. T. Goennenwein, Appl. Phys. Lett. **112**, 132401 (2018).
[9] P. Muduli, R. Schlitz, T. Kosub, R. Hübner, A. Erbe, D. Makarov, and S. T. Goennenwein, APL Mater. **9**, 021122 (2021).
[10] M. Street, W. Echtenkamp, T. Komesu, S. Cao, P. A. Dowben, and C. Binek, Appl. Phys. Lett. **104**, 222402 (2014).
[11] P. Appel, B. J. Shields, T. Kosub, N. Hedrich, R. Hübner, J. Faßbender, D. Makarov, and P. Maletinsky, Nano Lett. **19**, 1682 (2019).
[12] M. S. Wörnle, P. Welter, M. Giraldo, T. Lottermoser, M. Fiebig, P. Gambardella, and C. L. Degen, Phys. Rev. B **103**, 094426 (2021).
[13] N. A. Spaldin, J. Exp. Theor. Phys. **132**, 493 (2021).
[14] M. Stengel, Phys. Rev. B **84**, 205432 (2011).
[15] N. Nakagawa, H. Y. Hwang, and D. A. Muller, Nat. Mater. **5**, 204 (2006).
[16] D. Vanderbilt and R. D. King-Smith, Phys. Rev. B **48**, 4442 (1993).
[17] N. A. Spaldin, M. Fechner, E. Bousquet, A. Balatsky, and L. Nordström, Phys. Rev. B **88**, 094429 (2013).
[18] X. He, Y. Wang, N. Wu, A. N. Caruso, E. Vescovo, K. D. Belashchenko, P. A. Dowben, and C. Binek, Nat. Mater. **9**, 579 (2010).
[19] M. Fechner, A. Sukhov, L. Chotorlishvili, C. Kenel, J. Berakdar, and N. A. Spaldin, Phys. Rev. Mater. **2**, 064401 (2018).
[20] E. J. Samuelsent, M. T. Hutchings, and G. Shirane, Physica **48**, 13 (1970).
[21] S. Shi, A. L. Wysocki, and K. D. Belashchenko, Phys. Rev. B **79**, 104404 (2009).
[22] G. Kresse and J. Furthmüller, Phys. Rev. B **54**, 11169 (1996).
[23] See Supplemental Material at http://link.aps.org/supplemental/10.1103/PhysRevLett.130.146701 for details of the density functional theory calculations, details of the Monte Carlo simulations, estimates of critical exponents for surface and bulk sublattice magnetization, data for calculating multipolization tensors in the local moment approximation, total DFT + U energy for nonpolar (001) chromia slab compared to polar (001) slab and discussion of the feasibility of synthesis of (001) chromia with an Fe monolayer. Supplemental Material includes Refs. [24–37].
[24] P. E. Blochl, Phys. Rev. B **50**, 17953 (1994).

[25] V. I. Anisimov, F. Aryasetiawan, and A. I. Lichtenstein, J. Phys. Condens. Matter **9**, 76603 (1997).
[26] S. L. Dudarev, G. A. Botton, S. Y. Savrasov, C. J. Humphreys, and A. P. Sutton, Phys. Rev. B **57**, 1505 (1998).
[27] K. L. Dudko, V. V. Eremenko, and L. M. Semenenko, Phys. Status Solidi (b) **43**, 471 (1971).
[28] D. Tobia, E. D. Biasi, M. Granada, H. E. Troiani, G. Zampieri, E. Winkler, and R. D. Zysler, J. Appl. Phys. **108** (2010).
[29] H. J. Xiang, E. J. Kan, S. H. Wei, M. H. Whangbo, and X. G. Gong, Phys. Rev. B **84**, 224429 (2011).
[30] G. V. D. Laan, J. Phys. Condens. Matter **10**, 3239 (1998).
[31] P. Landau and K. Binder, *A Guide to Monte Carlo Simulations in Statistical Physics* (Cambridge University Press, Cambridge, England, 2005).
[32] S. Idrissi, S. Ziti, H. Labrim, and L. Bahmad, J. Mater. Eng. Perform. **29**, 7361 (2020).
[33] F. Rohr, M. Baumer, H.-J. F. A., J. A. Mejias, V. Staemmler, S. Miiller, L. Hammer, and K. Heinz, Surface Sci. **372**, L291 (1997).
[34] M. Bendert, D. Ehrlicht, I. N. Yakovkints, F. Rohrt, M. Baumert, H. Kuhlenheckt, H.-J. Freundt, and V. Staemmlert, J. Phys. Condens. Matter **7**, 5289 (1995).
[35] M. Lübbe and W. Moritz, J. Phys. Condens. Matter **21**, 134010 (2009).
[36] O. Bikondoa, W. Moritz, X. Torrelles, H. J. Kim, G. Thornton, and R. Lindsay, Phys. Rev. B **81**, 205439 (2010).
[37] T. C. Kaspar, S. E. Chamberlin, and S. A. Chambers, Surface Sci. **618**, 159 (2013).
[38] A. Urru and N. A. Spaldin, Ann. Phys. (Amsterdam) **447**, 168964 (2022).
[39] M. Mostovoy, A. Scaramucci, N. A. Spaldin, and K. T. Delaney, Phys. Rev. Lett. **105**, 087202 (2010).
[40] B. Skubic, J. Hellsvik, L. Nordström, and O. Eriksson, J. Phys. Condens. Matter **20**, 315203 (2008).
[41] A. L. Wysocki, S. Shi, and K. D. Belashchenko, Phys. Rev. B **86**, 165443 (2012).
[42] Y. Kota, H. Imamura, and M. Sasaki, Appl. Phys. Express **6**, 113007 (2013).
[43] H. Wang, C. Du, P. C. Hammel, and F. Yang, Phys. Rev. B **91**, 220410(R) (2015).
[44] L. Fallarino, E. L. Rojo, M. Quintana, J. S. S. Gallo, B. J. Kirby, and A. Berger, Phys. Rev. Lett. **127**, 147201 (2021).
[45] P. Borisov, A. Hochstrat, X. Chen, W. Kleemann, and C. Binek, Phys. Rev. Lett. **94**, 117203 (2005).
[46] Y. Kota, H. Imamura, and M. Sasaki, IEEE Trans. Magn. **50**, 1 (2014).
[47] Y. S. Dedkov, C. Laubschat, S. Khmelevskyi, J. Redinger, P. Mohn, and M. Weinert, Phys. Rev. Lett. **99**, 047204 (2007).
[48] G. Rosenberg and M. Franz, Phys. Rev. B **85**, 195119 (2012).
[49] S. Schulz, I. A. Nechaev, M. Güttler, G. Poelchen, A. Generalov, S. Danzenbächer, A. Chikina, S. Seiro, K. Kliemt, A. Y. Vyazovskaya, T. K. Kim, P. Dudin, E. V. Chulkov, C. Laubschat, E. E. Krasovskii, C. Geibel, C. Krellner, K. Kummer, and D. V. Vyalikh, npj Quantum Mater. **4**, 26 (2019).
[50] S. Mu, A. L. Wysocki, and K. D. Belashchenko, Phys. Rev. B **87**, 054435 (2013).
[51] A. Mahmood, W. Echtenkamp, M. Street, J. L. Wang, S. Cao, T. Komesu, P. A. Dowben, P. Buragohain, H. Lu, A. Gruverman, A. Parthasarathy, S. Rakheja, and C. Binek, Nat. Commun. **12**, 1674 (2021).